Mean-Flow Damping Forms the Buffer Zone of the Quasi-Biennial Oscillation: 1D Theory

AARON MATCH

Program in Atmospheric and Oceanic Sciences, Princeton University, Princeton, New Jersey

STEPHAN FUEGLISTALER

Department of Geosciences, and Program in Atmospheric and Oceanic Sciences, Princeton University, Princeton, New Jersey

(Manuscript received 17 October 2019, in final form 18 March 2020)

ABSTRACT

The quasi-biennial oscillation (QBO) is a descending pattern of alternating easterly and westerly winds in the tropical stratosphere. Upwelling is generally understood to counteract the descent of the QBO. The *upwelling hypothesis* holds that where upwelling exceeds the intrinsic descent rate of the QBO, the QBO cannot descend and a buffer zone forms. Descent-rate models of the QBO, which represent a highly simplified evolution of a QBO wind contour, support the upwelling hypothesis. Here, we show that the upwelling hypothesis and descent-rate models only correctly describe buffer zone formation in the absence of wave dissipation below critical levels. When there is wave dissipation below critical levels, the 1D QBO response to upwelling can be either to 1) reform below the upwelling, 2) undergo period-lengthening collapse, or 3) expand a preexisting buffer zone. The response depends on the location of the upwelling and the lower boundary condition. Mean-flow damping always forms a buffer zone. A previous study of reanalyses showed that there is mean-flow damping in the buffer zone due to horizontal momentum flux divergence. Therefore, the 1D model implicates lateral terms in buffer zone formation that it cannot self-consistently include.

1. Introduction

The quasi-biennial oscillation (QBO) is a descending pattern of alternating easterly and westerly winds in the tropical stratosphere with an average period of 28 months. The QBO is driven by interactions between the mean flow and a wide spectrum of vertically propagating waves, from planetary-scale Kelvin and mixed Rossby–gravity waves to small-scale gravity waves.

The classical theory of the QBO is based on a one-dimensional (1D) model of the tropical stratosphere with a source of parameterized waves at the tropopause (Holton and Lindzen 1972). The 1D models of the QBO have yielded insights into its descent mechanism and period (Plumb 1977; Dunkerton 1981), and continue to guide interpretations of QBO dynamics in general circulation models (GCMs) (e.g., Hamilton et al. 1999; Kawatani et al. 2011; Anstey et al. 2016).

A key application of 1D models is to study interactions between upwelling and the QBO. Upwelling is understood to resist the descent of the QBO. Early accounts of the resistive effects of tropical mean upwelling on the QBO led to upward revisions of the wave stress required to drive the QBO (Gray and Pyle 1989; McIntyre 1994; Dunkerton 1997). Variability in upwelling also drives variability in the QBO descent rate. The annual cycle in upwelling has been linked to observed weak phase-locking of the QBO with the annual cycle (Hampson and Haynes 2004; Rajendran et al. 2016). In this paper, we consider how upwelling impacts the QBO without considering the consequences of anomalous upwelling induced by the secondary circulation of the QBO.

This paper revisits the problem of whether and how climatological upwelling can form a buffer zone. A buffer zone is a region where the QBO would exist were it not for dynamical interference by processes unrelated to the QBO (Match and Fueglistaler 2019). Saravanan (1990) showed that a bottom-heavy upwelling profile representing the top of the Hadley cell appears to form a buffer zone between the lower extent of the QBO and the wave source. The buffer zone filters the waves that propagate into the QBO region (Saravanan 1990). The buffer zone arguably plays an important role

Corresponding author: Aaron Match, amatch@princeton.edu

DOI: 10.1175/JAS-D-19-0293.1

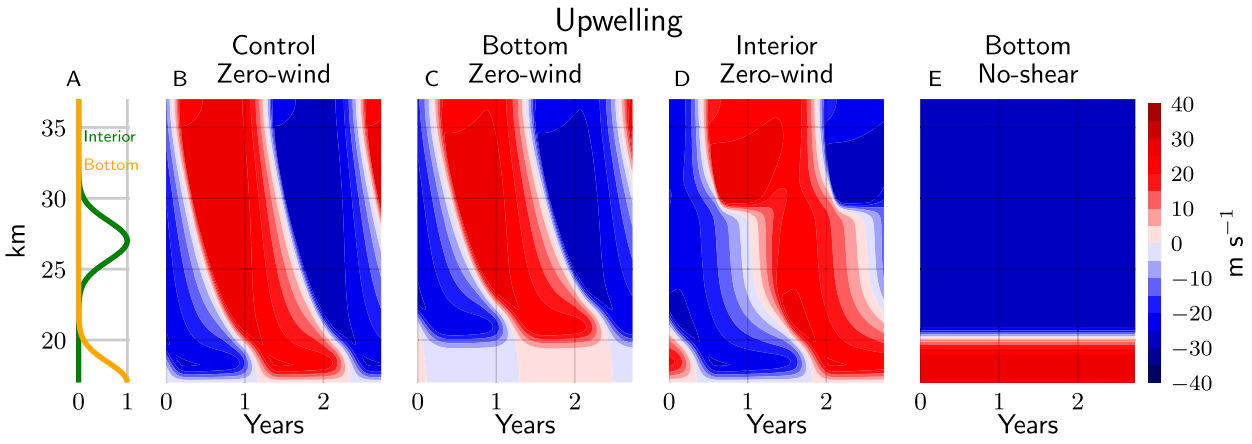

FIG. 1. The response of the 1D model of the QBO (described in the appendix) to localized upwelling perturbations using the P77 wave drag formulation. (a) Vertical structure of perturbations normalized by maximum value. (b) Control simulation (i.e., with zero upwelling) and zero-wind lower boundary condition. (c) With bottom upwelling and a zero-wind lower boundary condition, there is an expanded buffer zone as in Saravanan (1990). (d) With interior upwelling and a zero-wind lower boundary condition, the QBO reforms below the upwelling. (e) With bottom upwelling and a no-shear lower boundary condition, the QBO undergoes period-lengthening collapse. The upwelling is Gaussian with a decay scale of 2 km and a peak magnitude of 2 mm s^{-1}, and it is centered in the interior (27 km) or at the bottom (17 km).

in dynamical linkages between the QBO and tropical weather, such as the proposed connection between the QBO and tropical convection associated with the Madden–Julian oscillation (Yoo and Son 2016; Martin et al. 2019).

Saravanan (1990) hypothesized that the top of the buffer zone forms where upwelling balances the wave-driven descent rate of the QBO. Saravanan's upwelling hypothesis for buffer zone formation continues to guide understanding of the basic state of the buffer zone and interpretations of its trends in response to global warming (e.g., Kawatani et al. 2011; Kawatani and Hamilton 2013; Richter et al. 2020). Zero-dimensional *descent-rate models* of the QBO, which have added a lower rung to the hierarchy of QBO models, also support the upwelling hypothesis. Descent-rate models make restrictive assumptions about the QBO vertical structure in order to represent the descent of QBO features locally. Both the upwelling hypothesis and descent-rate models treat QBO features as objects that are advected by the local wave drag and upwelling.

We will show that the advective perspective of QBO descent only strictly applies when there is no wave dissipation below critical layers, as in the wave drag formulation of Lindzen and Holton (1968, hereafter LH68). If there is wave drag below critical layers, as in the wave drag formulation of Plumb (1977, hereafter P77), then the QBO response to upwelling cannot be described by advective arguments. When advective arguments fail, the QBO response to upwelling depends on the location of the upwelling and the lower boundary condition. Figure 1 shows the 1D QBO response to upwelling under various model configurations. [The 1D model is described in the appendix including the 1D model equation, Eq. (A1), with parameters in Table 1.] Figure 1c shows the canonical buffer zone in experiments with upwelling at the bottom of a domain and a zero-wind lower boundary condition, as in Saravanan (1990). Upwelling has previously been understood to form a buffer zone in this experiment, but we argue that upwelling is instead expanding the pre-existing buffer zone that is imposed by the zero-wind lower boundary condition. Depending on the location of the upwelling and the lower boundary condition, the QBO can also reform below the upwelling (Fig. 1d) or undergo period-lengthening collapse (Fig. 1e).

In this paper, we introduce the advective framework for the response of QBO features to upwelling, as exemplified by the upwelling hypothesis for buffer zone formation, descent-rate models, and the LH68 wave drag (section 2). Then, we describe the nonlocal dynamics that occur when there is wave dissipation below critical layers, as in the P77 wave drag (section 3). When there is wave dissipation below critical levels, the QBO will be shown to respond to upwelling by either 1) reforming below the upwelling, 2) undergoing period-lengthening collapse, or 3) expanding the buffer zone. We explain the dynamics of each of these responses and the model configurations that lead to each one. The upwelling hypothesis for buffer zone formation will be shown to not be robust to model configuration choices. On the other hand, mean-flow damping robustly forms a buffer zone (section 4). These results harmonize with Match and Fueglistaler (2019), which implicated mean-flow damping by horizontal momentum flux divergence in forming the buffer zone.

TABLE 1. Parameter values for 1D model simulations.

Parameter	Description	Value
ρ_L	Density at z_L	$1\,\mathrm{kg\,m^{-1}}$
H_ρ	Density scale height	7 km
ν	Diffusivity	$0.3\,\mathrm{m^2\,s^{-1}}$
F_L	Wave momentum flux (P77)	$0.01\,\mathrm{m^2\,s^{-2}}$
N	Buoyancy frequency (P77)	$2.16\times10^{-2}\,\mathrm{s^{-1}}$
μ	Wave dissipation rate (P77)	$10^{-6}\,\mathrm{s^{-1}}$
k	Wavenumber (P77)	$2\pi/40\,000\,\mathrm{km^{-1}}$
c	Wave phase speed (P77)	$30\,\mathrm{m\,s^{-1}}$
f	Wave momentum flux density (LH68)	$2\times10^{-4}\,\mathrm{kg\,s^{-1}}$

2. The QBO response to upwelling without background wave dissipation

Saravanan (1990) is the first paper to explicitly investigate the dynamics of the QBO buffer zone. Saravanan argued that a buffer zone forms in a 1D model of the QBO when there is an exponentially decreasing upwelling profile above the model's zero-wind lower boundary condition. We reproduce the upwelling buffer zone (using a Gaussian upwelling profile) in Fig. 1c. Saravanan argued that the buffer zone is formed by upwelling, which we call the *upwelling hypothesis*. The upwelling hypothesis continues to prevail today. The upwelling hypothesis can be represented by the following implicit equation (Saravanan 1990, p. 2472):

$$\overline{w}^*(z_b) \approx f(\overline{u}), \tag{1}$$

which states that the residual upwelling $\overline{w}^*$ at the top of the buffer zone balances the wave-driven descent rate of the QBO f as a function of the wind at the top of the buffer zone. The upwelling hypothesis fits into a common perspective that QBO features are advected downward by the wave drag. The advective perspective of the QBO wave drag culminates in *descent-rate models* of the QBO (introduced in this section). Yet, wave drag is advective only when it is proportional to the vertical zonal wind shear. One wave drag formulation proportional to vertical shear is LH68, which assumes a continuous spectrum of waves dissipating only at critical levels (Campbell and Shepherd 2005a). In the next section, we show that when the wave drag is not advective (which occurs when the assumptions of LH68 are relaxed), the predictions from the upwelling hypothesis break down.

The LH68 wave drag assumes a continuous spectrum of vertically propagating waves that only dissipate at critical levels, where $\overline{u} = c$. Each infinitesimal band of phase speed dc contains infinitesimal wave momentum flux $f(c)dc$. (The wave momentum flux density with respect to phase speed f will be shown to be proportional to the wave-driven descent rate f in the LH68 wave drag formulation, which is why the symbol f is used for both). The wave momentum flux F that diverges in a vertical layer $[z, z+\Delta z]$ that has winds in the range $[\overline{u}, \overline{u}+\Delta\overline{u}]$ is proportional to the wave momentum flux density in phase speed space integrated across all critical levels in that layer (assuming there is no wave dissipation below): $F(z) - F(z+\Delta z) = \int_{\overline{u}}^{\overline{u}+\Delta\overline{u}} f(u)\,du$. Assuming that the wave momentum flux density is constant (i.e., independent of phase speed) and taking limits, the LH68 wave drag G_{LH68} equals the following:

$$G_{\mathrm{LH68}} = -\frac{1}{\rho_0}\frac{dF}{dz} = \frac{f}{\rho_0}\frac{\partial\overline{u}}{\partial z}, \tag{2}$$

with base-state density $\rho_0 = \rho_L \exp[-(z - z_L)/H_\rho]$, density-scale height H_ρ, and the lower boundary indicated by subscript L. The wave drag is proportional to the vertical shear, so it operates as a vertical advection with speed f/ρ_0. Note that the LH68 wave drag advects zonal momentum, but not other tracers.

The advective motion of QBO features in the LH68 wave drag suggests that a *descent-rate model* could be produced that tracks a particular QBO feature as it descends through the stratosphere subject to the effects of upwelling and wave drag. A descent-rate equation is constructed by dividing the prognostic equation for zonal wind $\partial\overline{u}/\partial t$ by minus the vertical shear $\partial\overline{u}/\partial z$ (Dunkerton 1991; Dunkerton and Delisi 1997; Dunkerton 2000; Rajendran et al. 2018). To represent QBO processes locally, restrictive assumptions must be made about the structure of the wind away from the feature of interest. A descent-rate equation is transformed into a descent-rate model by implementing heuristic representations of stalling, annihilation, and reformation aloft of each QBO shear zone.

We now briefly construct a descent-rate model for the LH68 wave drag parameterization that demonstrates how descent-rate models support the upwelling hypothesis for buffer zone formation. Consider a simplified version of the full 1D QBO model [Eq. (A1)]:

$$\frac{\partial\overline{u}}{\partial t} = G + \frac{1}{\rho_0}\frac{\partial}{\partial z}\left(\rho_0\nu\frac{\partial\overline{u}}{\partial z}\right) - \overline{w}^*\frac{\partial\overline{u}}{\partial z}. \tag{3}$$

The terms on the right-hand side are wave drag, vertical diffusion, and upwelling, with time t, height z, zonal wind u, wave drag resulting from the dissipation of vertically propagating waves in the QBO winds G, vertical diffusivity ν, and climatological residual vertical velocity $\overline{w}^*$. [Note that Eq. (3) matches the full 1D model, Eq. (A1), except without mean-flow damping or prescribed acceleration.]

The following LH68 descent-rate equation for the zero-wind level z_0 can be constructed by assuming 1) constant density, 2) a no-shear lower boundary condition, 3) negligible diffusion near the zero-wind level,[1] and 4) that the wave drag at z_0 is not dissipated by critical levels below z_0:

$$\frac{dz_0}{dt} = \overline{w}^*(z_0) - f. \tag{4}$$

The descent-rate equation suggests that the zero wind line is advected by the summed effects of upwelling and wave drag. Upwelling always appears alone in descent-rate equations (because they are derived by dividing vertical advection $-\overline{w}^*\overline{u}_z$ by minus the vertical shear $-\overline{u}_z$). Importantly, the descent rate due to the LH68 wave drag only appears so simply because the LH68 wave drag is proportional to the vertical shear [Eq. (2)]. In section 3, we analyze a wave drag that does not act like advection, and therefore cannot be emulated by a descent-rate model.

The descent-rate model tracks two zero-wind levels: one with positive vertical shear and one with negative vertical shear. Descent-rate models assume that these zero-wind levels move continuously when in the interior of the domain. Only at predetermined locations are these zero-wind levels assumed to be annihilated and reformed. In the LH68 descent-rate model, the zero-wind level is assumed to descend until it reaches $z = 0$, at which level it annihilates the previously stalled shear zone, then stalls. When a shear zone is annihilated, it is assumed to reform immediately at the top of the domain.[2]

The LH68 descent-rate model suggests that the zero-wind level moves downward if the upwelling $\overline{w}^*$ is less than the wave-driven descent rate f. If the upwelling balances the wave-driven descent rate, then the zero-wind level stalls indefinitely. If the upwelling exceeds the wave-driven descent rate, then QBO features ascend. Figure 2 shows the results from integrating the LH68 descent-rate model in a control experiment with no upwelling versus in a perturbation experiment with large, localized upwelling centered in the middle of the domain. With large interior upwelling, the QBO stalls

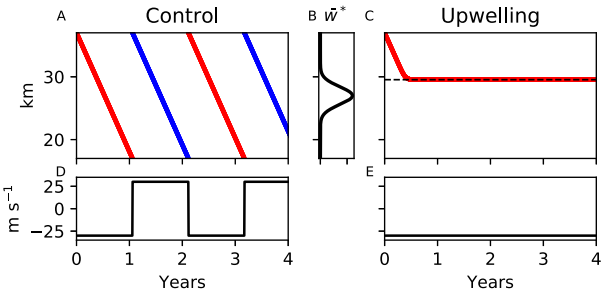

FIG. 2. Descent-rate model with LH68 wave drag formulation. (a) Control experiment with zero upwelling. The descent-rate model evolves the location of the zero-wind line with $\overline{u}_z < 0$ (blue) and the zero-wind line with $\overline{u}_z > 0$ (red). (b) Vertical structure of upwelling perturbation, which is Gaussian with an amplitude of 3 mm s^{-1} centered at 27 km with a decay scale of 2 km. (c) Experiment with upwelling imposed from (b). The zero-wind level stalls indefinitely where upwelling balances the wave-driven descent rate. (d) Zonal wind at the lower boundary in control experiment. (e) Zonal wind at the lower boundary in the upwelling experiment. In both cases, the wave-driven descent rate $f = 0.6$ mm s^{-1} and the background density in constant. The model is integrated using the first-order Euler method.

indefinitely at the level where upwelling cancels the wave-driven descent (Fig. 2b), consistent with the upwelling hypothesis [Eq. (1)].

Using the LH68 wave drag formulation, upwelling can form a buffer zone in the 1D model just as predicted by the upwelling hypothesis and the descent-rate model. Figure 3c shows the buffer zone formed by upwelling using the LH68 wave drag formulation. The model parameters are described in Table 1. The top of the buffer zone matches the prediction from the upwelling hypothesis.

In the LH68 wave drag, the descent rate of shear zones reduces to a simple balance between wave-driven descent rate and upwelling, owing to the advective form of the wave drag. Descent-rate models assume that wave drag leads only to continuous motion of QBO features in the interior of the domain, which leads these models to corroborate the upwelling hypothesis. The next section shows that if waves dissipate before reaching their first critical level, then wave drag can act differently than downward advection, and QBO features can move discontinuously.

3. The QBO response to upwelling with background wave dissipation

Hypotheses about the QBO response to upwelling that do not account for dissipation below critical levels fail to describe QBO dynamics when there is wave dissipation below critical levels. We analyze QBO responses to upwelling using the canonical P77 wave drag

[1] Diffusion vanishes at z_0 if the wind is an odd function of height in the vicinity of z_0 [i.e., $\overline{u}(z_0 + dz) = -\overline{u}(z_0 - dz)$].

[2] Because the LH68 shear zone cannot initiate a shear zone without contributions from external accelerations, which are typically assumed to come in the form of a semiannual oscillation, the assumption that a new shear zone forms *immediately* is tantamount to assuming that there is an externally forced oscillation at the top of the domain with a much higher frequency than that of the QBO.

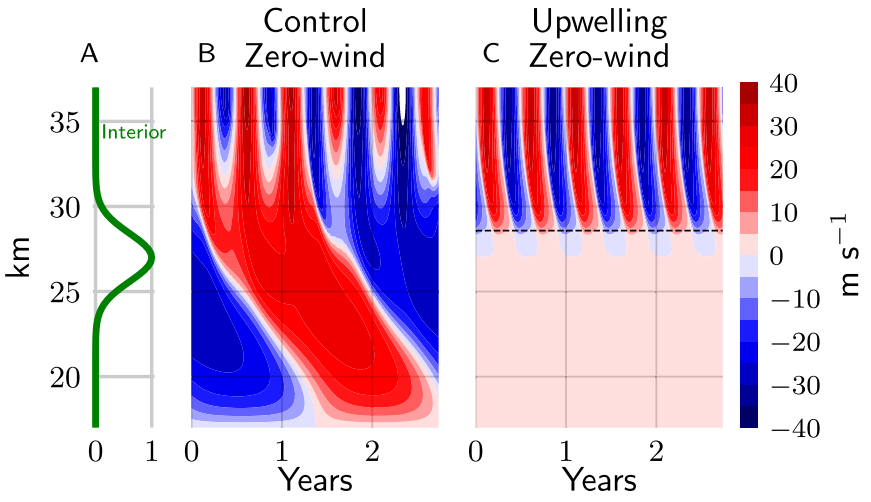

FIG. 3. Interior upwelling forms a buffer zone in the 1D LH68 QBO. (a) Vertical structure of perturbations normalized by maximum value. (b) Control experiment. (c) Upwelling experiment with Gaussian upwelling centered at 27 km with an amplitude of 2 mm s^{-1} and a decay scale of 2 km. Using the LH68 wave drag formulation, upwelling forms a buffer zone from z_b^+ (marked with the black dashed line) to the bottom of the domain. The LH68 QBO requires prescribed acceleration X to initiate shear zones, which takes the form of a semiannual oscillation near the top of the domain (described in the appendix).

formulation, which is arguably the simplest wave drag formulation with wave dissipation below critical levels.

a. *P77 wave drag*

The P77 wave drag assumes two discrete vertically propagating waves of equal and opposite phase speed that experience constant radiative or mechanical dissipation. As the waves dissipate, they accelerate the wind toward their phase speed. The vertical group velocity of the waves depends nonlinearly on the difference between the phase speed of the wave and the mean flow. If the vertical group velocity is small, then the wave moves slowly and a large amount of dissipation occurs over a shallow vertical extent. P77 waves are assumed to have the dispersion relation of gravity waves or Kelvin waves, which relates the vertical group velocity of the wave to the background wind.[3] For gravity waves or Kelvin waves, the vertical group velocity is $c_{gz} = k(u - c_n)^2/N$, with buoyancy frequency N, wavenumber k, and phase speed c for discrete wave n. The P77 parameters are listed in Table 1. Assuming a constant wave dissipation rate μ, the wave momentum flux as a function of height for a wave with source momentum flux F_L equals

$$F_n(z) = \rho_L F_L \mathrm{sgn}(c_n) \exp\left(-\int_{z_L}^{z} \frac{\mu}{c_{gz}} dz'\right). \quad (5)$$

The wave drag is proportional to the wave momentum flux divergence summed across all waves:

$$G_{\mathrm{P77}} = -\frac{1}{\rho_0} \sum_n \frac{\partial F_n}{\partial z}. \quad (6)$$

The P77 wave drag at a given level depends nonlocally on the winds at that level and between that level and the wave source. In contrast to the LH68 wave drag, the P77 wave drag does not depend on the winds above that level or on the vertical shear (P77; Campbell and Shepherd 2005a). Because the P77 wave drag is not proportional to the vertical shear, it is not advective. Transforming the P77 wave drag into a descent-rate equation does not simplify it, and consequently the P77 descent-rate model fails to emulate the response of the 1D P77 QBO to large upwelling.

Whereas the LH68 QBO forms a buffer zone below large upwelling, the P77 QBO will be shown to exhibit three types of responses to upwelling depending on the location of the upwelling and the lower boundary condition. These three responses were shown in Fig. 1, and the dynamics of each will be discussed in the following

[3] In the first 1D model of the QBO, Holton and Lindzen (1972) considered an asymmetric situation with one eastward-propagating Kelvin wave and one westward-propagating Rossby wave. We adopt the symmetrical approach of Plumb (1977) by assuming waves of equal and opposite phase speed with identical dispersion relations. If these waves are assumed to be Kelvin waves, then the westward-propagating "anti-Kelvin" wave is unphysical. Gravity waves of equal and opposite phase speeds are physically realizable.

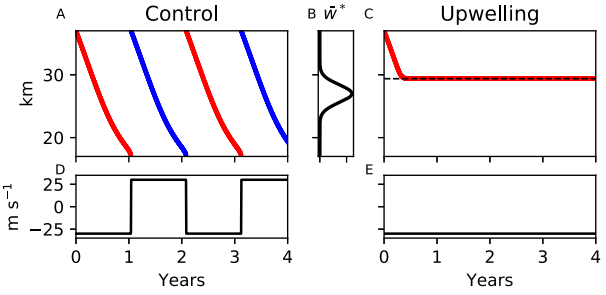

FIG. 4. As in Fig. 2, but for a descent-rate model using the P77 wave drag formulation. (a) Control experiment with zero upwelling. (b) Vertical structure of upwelling perturbation, which is Gaussian with an amplitude of 3 mm s^{-1} centered at 27 km with a decay scale of 2 km. (c) Upwelling experiment during which the zero-wind level stalls indefinitely when it reaches the level where upwelling balances the wave-driven descent rate. (d) Zonal wind at the lower boundary in control experiment. (e) Zonal wind at the lower boundary in upwelling experiment. The descent-rate model implementation follows Rajendran et al. (2018) except here the model upper boundary is 37 km. The wave forcing F is 0.05 m^2 s^{-2}.

order: 1) reformation below the upwelling perturbation (Fig. 1d), 2) period-lengthening collapse (Fig. 1e), and 3) expansion of the buffer zone (Fig. 1c).

b. *Reformation below the upwelling perturbation*

The P77 wave drag at a given level does not depend on the flow above that level, which poses the following challenge to the upwelling hypothesis for buffer zone formation: Consider that a large-amplitude, localized upwelling perturbation is imposed in the interior of the P77 QBO. The upwelling hypothesis and descent-rate models suggest that a buffer zone should form below the level where the upwelling balances the descent rate of the QBO. (The descent-rate model prediction for the P77 wave drag, based on the descent-rate model of Rajendran et al. (2018) is shown in Fig. 4, which makes an identical prediction for the response of the QBO to upwelling as does the LH68 descent-rate model in Fig. 2. Yet, in terms of the P77 wave drag, the QBO below the large upwelling perturbation should evolve as if the perturbation was never imposed.

Figure 1d shows the response of the 1D P77 QBO to large interior upwelling. Counter to the prediction from the descent-rate model with P77 wave drag, no buffer zone forms when the 1D P77 QBO is subject to large interior upwelling. Instead, the flow below the upwelling perturbation evolves as if the perturbation was not imposed. Descent-rate models fail to emulate the 1D P77 QBO response to large upwelling because they assume that the motion of QBO features is continuous and can be emulated by advection. Because the P77 wave drag is not proportional to vertical shear and is not advective, the advective framework fails to describe the response of the P77 QBO to upwelling. In particular, the advective framework precludes the possibility of QBO features reforming below a perturbation. Not only does the QBO reform below the upwelling perturbation, but upwelling does not even attenuate the QBO in the perturbed region.

It is useful to clarify the dynamics that are occurring in Fig. 1d. The wave-driven descent rate is balanced by the perturbation upwelling near the top of the upwelling perturbation at approximately 29 km (z_b^+) and near the bottom of the upwelling perturbation at approximately 25 km (z_b^-). Between z_b^- and z_b^+, the upwelling exceeds the wave-driven QBO descent rate and QBO features move upward, becoming virtually homogeneous and approximately synchronized with the winds at z_b^-. Above z_b^+ or below z_b^-, QBO features descend due to the wave drag. Because the P77 wave drag does not depend on the winds aloft, the wind evolution near z_b^- is similar to that which would have occurred in the absence of the upwelling perturbation. Therefore, the winds that would have formed at z_b^- anyway in a control experiment are rapidly advected upward by the upwelling. The result is that the winds in the strong upwelling region are not attenuated, but rather oscillate with a phase lag relative to that which would have occurred in the control. The phase lag increases with the height above z_b^-, maximizing just below z_b^+.

The P77 QBO can only reform below perturbations if there is enough space for a new shear zone to form. If the upwelling is imposed near the lower boundary condition, then z_b^- will coincide with the lower boundary. Then, rather than filling in properties that match what would have occurred in a control experiment, the upwelling will fill in properties that depend strongly on the lower boundary condition. The next two examples of P77 QBO responses to upwelling represent the responses when the upwelling perturbations abut the lower boundary condition.

c. *Period-lengthening collapse*

If upwelling is imposed at the bottom of the QBO domain with a no-shear lower boundary condition, then as the amplitude of the upwelling is increased, the period of the QBO increases. After the QBO period diverges to infinity, the system locks into a steady state. We characterize this route to collapse as *period-lengthening collapse*. Figure 1e shows one example of such a steady state. The steady state wind profile depends on the initial conditions.

The steady state emerges because the upwelling prolongs the stalling stage of the QBO cycle. Once the upwelling causes the QBO to stall indefinitely,

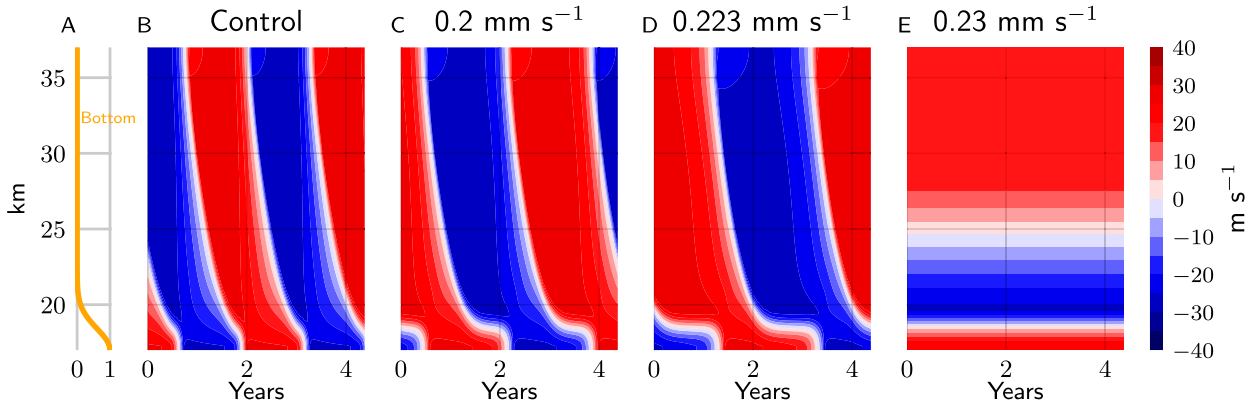

FIG. 5. Response of the 1D P77 QBO to bottom upwelling with a no-shear lower boundary condition. (a) The upwelling perturbation is Gaussian with a decay scale of 2 km. (b) Control experiment with zero upwelling. Upwelling with a magnitude of (c) 0.2 mm s^{-1} and (d) 0.223 mm s^{-1} lengthens the stalling at the lower boundary. (e) Upwelling with a magnitude of 0.23 mm s^{-1} leads to period-lengthening collapse of the QBO.

the system locks. The locked state represents a dynamic equilibrium, such that if the upwelling were turned off, the system would resume oscillating.

The details of the momentum balance in the locked state depend on the wind structure, which in turn depends on the initial conditions. For the locked state shown in Fig. 1e, the momentum balance is characterized as follows: The westerly P77 wave dissipates near the lower boundary. Below the zero-wind line, westerly momentum is advected upward by the upwelling and is balanced by diffusion. Above the zero-wind line, easterly wave drag is balanced by diffusion.

Collapse of the QBO appears to occur once the upwelling exceeds the wave-driven descent rate somewhere near the lower boundary. Figure 5 shows some steps on the approach toward period-lengthening collapse. As the upwelling is increased, the QBO period increases nonlinearly. Between $\overline{w}^* = 0.222$ mm s^{-1} (Fig. 5d) and $\overline{w}^* = 0.23$ mm s^{-1} (Fig. 5e), the period diverges to infinity and the oscillation collapses. Figure 6 shows that the oscillation collapses when the upwelling first exceeds the descent rate of the control QBO, about 1.25 km above the lower boundary. In this case, the upwelling exceeds the descent rate between 18 and 19 km, which is the minimum in the QBO descent rate, and corresponds to the levels where the descending shear zone tends to slow as it interacts diffusively with the stalled shear zone below.

d. Expansion of the buffer zone

Since zero-wind lower boundary conditions are standard practice in 1D QBO modeling, it might be assumed that the amplitude of the 1D QBO inevitably goes to zero at the wave source. Yet, with a no-shear lower boundary condition, the QBO maintains large amplitude down to the wave source (Fig. 5b). Since quiescent winds at or near the wave source are not inevitable consequences of the QBO descent mechanism, they must be explained in terms of a buffer zone formation mechanism. A zero-wind lower boundary condition is tantamount to prescribing a buffer zone.

Because the simulations in support of the upwelling hypothesis use a zero-wind lower boundary condition (i.e., a prescribed buffer zone), those simulations do not demonstrate how to form a buffer zone, but how to expand a preexisting buffer zone. Upwelling expands the buffer zone by advecting zero wind upward from the

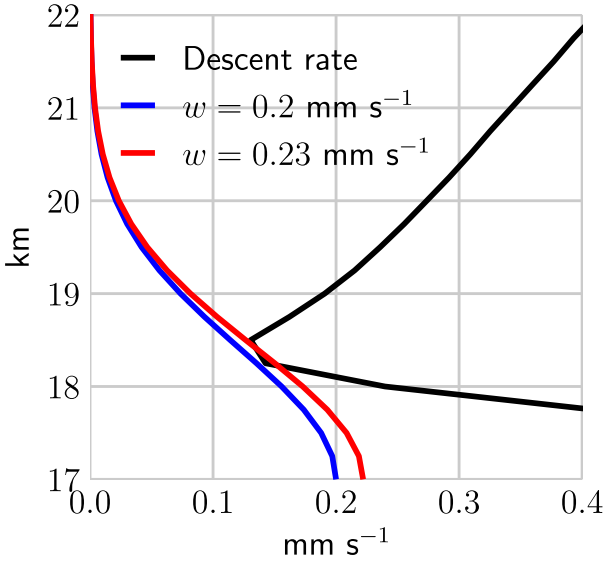

FIG. 6. Profiles of bottom upwelling with magnitudes of 0.2 mm s^{-1} (blue, as in Fig. 5c) and 0.23 mm s^{-1} (red, as in Fig. 5e). Descent rate (black) from the control P77 simulation with no-shear lower boundary condition (Fig. 5b). When upwelling exceeds the descent rate (i.e., red intersects black), the QBO has undergone period-lengthening collapse as shown in Fig. 5e.

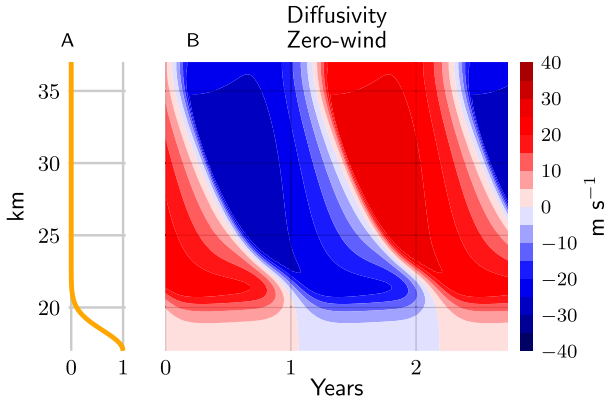

FIG. 7. The 1D QBO simulation with enhanced diffusivity at the bottom of the domain. Enhanced diffusivity adds a Gaussian diffusivity profile with a peak amplitude of 3 $m^2 s^{-1}$ centered at 17 km with a decay scale of 2 km to the background diffusivity of 0.3 $m^2 s^{-1}$. Enhanced diffusivity expands the buffer zone in a virtually identical way as upwelling does (Fig. 1c).

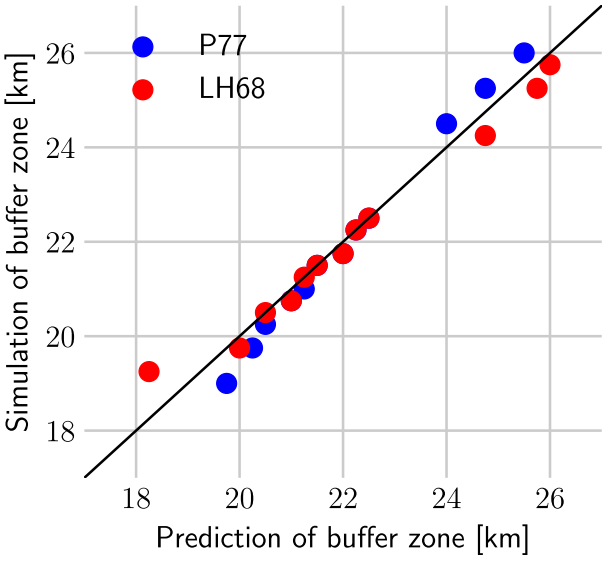

FIG. 8. Simulated top of buffer zone in 1D model vs predicted top of buffer zone for a range of Gaussian upwelling profiles imposed at a zero-wind lower boundary condition. The upwelling perturbations have different amplitudes and decay scales. The simulated top of the buffer zone is defined where the standard deviation of the wind drops below 5 m s^{-1}. The predicted top of the buffer zone occurs at the highest level where upwelling balances the wave-driven descent rate, where the wave-driven descent rate is calculated in a control experiment without upwelling.

lower boundary (Fig. 1c). Upwelling is not unique in its ability to expand the buffer zone; any process that homogenizes the winds near a buffer zone expands the buffer zone. Figure 7 shows that enhanced vertical diffusivity near the lower boundary expands the buffer zone by diffusing zero wind upward from the lower boundary.

Numerous simulations with various magnitudes and height scales of upwelling reveal that upwelling expands the buffer zone up to the level z_b^+ where upwelling balances the wave-driven descent rate from the control simulation. Figure 8 summarizes these results for both the LH68 and P77 wave drag. In experiments with the LH68 wave drag, upwelling forms the buffer zone (as shown in Fig. 3c). In experiments with the P77 wave drag and a zero-wind lower boundary condition, the zero-wind lower boundary condition prescribes the buffer zone and upwelling expands it to z_b^+.

4. A new hypothesis for buffer zone formation

The upwelling hypothesis correctly describes buffer zone formation only when there is no wave dissipation below critical levels, as in the LH68 wave drag formulation. When there is critical-level dissipation below critical levels, as in the P77 wave drag formulation, the upwelling hypothesis fails. Upwelling cannot form a buffer zone, but can only expand a preexisting buffer zone. Furthermore, upwelling is not unique in its ability to expand a preexisting buffer zone; enhanced diffusivity can, too.

An alternative hypothesis for buffer zone formation supported by the 1D model is that *mean-flow damping forms the buffer zone*. Mean-flow damping in the 1D model is represented by the term $-\kappa\overline{u}$ in Eq. (A1). Mean-flow damping is not expected in the stratosphere from first principles, yet has been diagnosed in the buffer zone and is therefore worth considering as a buffer zone formation mechanism. The manner in which three-dimensional stratospheric dynamics might produce mean-flow damping is considered further in the discussion.

Figure 9 shows that mean-flow damping can form a buffer zone regardless of the lower boundary condition or damping location. The buffer zones at the bottom of the domain match the conventional understanding that the top of the buffer zone coincides with the bottom of the QBO (Figs. 9b,c). The buffer zones in the interior of the domain test the nuances of the buffer zone definition (Figs. 9d,e). They are certainly quiescent, yet the QBO reforms below. Match and Fueglistaler (2019) defined the buffer zone as "the region where the QBO would exist were it not for interference by dynamical processes unrelated to the QBO." By their definition, the interior quiescent regions are buffer zones. Regardless of whether such a region is defined as a buffer zone, mean-flow damping distinguishes itself from upwelling or enhanced diffusivity by forming a quiescent region when imposed in the interior of the domain, as opposed to upwelling which merely shifts the phase of the QBO without diminishing its amplitude.

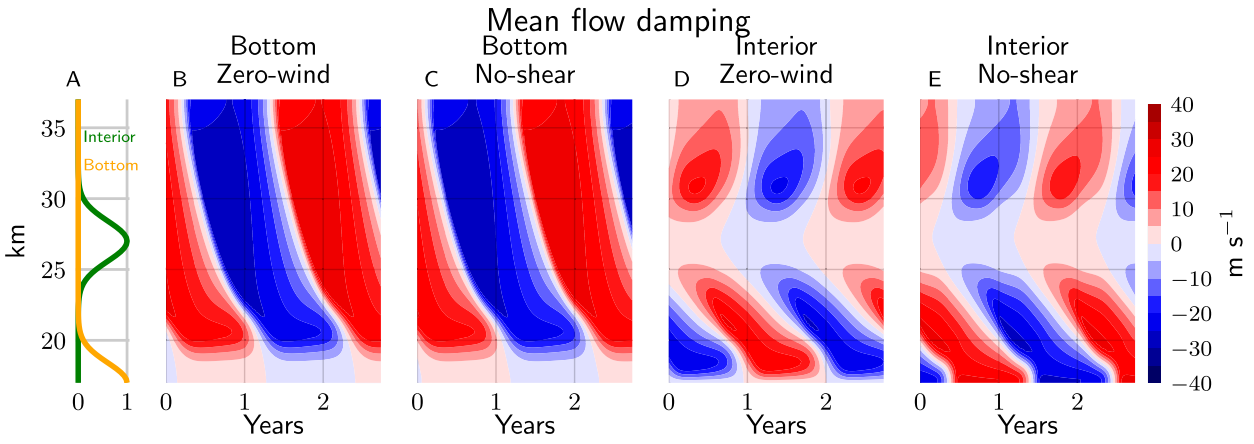

FIG. 9. Simulations using the 1D P77 QBO model with mean-flow damping imposed at various levels and with various lower boundary conditions. (a) Vertical structure of perturbations normalized by maximum value. (b) Mean-flow damping at the bottom of the domain with a zero-wind lower boundary condition. (c) Mean-flow damping at the bottom of the domain with a no-shear lower boundary condition. (d) Mean-flow damping in the interior of the domain with a zero-wind lower boundary condition. (e) Mean-flow damping in the interior of the domain with a no-shear lower boundary condition. Mean-flow damping profiles are Gaussian with a peak amplitude of $\kappa = 10^{-6}\,\mathrm{s}^{-1}$, centered at the bottom (17 km) or the interior (27 km), and a decay scale of 2 km. Mean-flow damping forms a buffer zone for all forcing locations and boundary conditions.

Mean-flow damping forms a buffer zone if the damping time scale is shorter than the QBO period. If the damping time scale is much longer than the QBO period, then the QBO can descend through the damping region without appreciable loss of amplitude. The mean-flow damping experiments in Fig. 9 have a mean-flow damping amplitude of $\kappa = 10^{-6}\,\mathrm{s}^{-1}$, which corresponds to a damping time scale of 12 days, much shorter than the QBO period.

5. Discussion

The upwelling hypothesis has been used to interpret buffer zone dynamics in observations and GCMs. Based on GCM simulations, Kawatani et al. (2011) proposed that increases in residual upwelling in the buffer zone associated with global warming could raise the top of the buffer zone. Kawatani and Hamilton (2013) reported an expansion trend in the top of the buffer zone in observations, which they attributed to an increasing trend in upwelling. The focus in Kawatani and Hamilton (2013) on upwelling—a process that expands the buffer zone—could be complemented in future studies by a focus on buffer zone formation processes.

QBO features in GCMs tend to be higher up in the stratosphere compared to in reanalyses. Typically, the pressure at which peak QBO amplitude occurs is 10 hPa in GCMs versus 20 hPa in reanalyses (Schenzinger et al. 2017). The pressure at the top of the buffer zone is typically 75 hPa in GCMs versus 85 hPa in reanalyses (Schenzinger et al. 2017). Recent explanations for the elevated buffer zone in QBO models focus on processes that drive the QBO; for example, the depth to which the QBO descends has been linked to the vertical resolution in the buffer zone, which is hypothesized to influence resolved wave driving of the QBO (Anstey et al. 2016; Geller et al. 2016). A complementary perspective to interpreting the elevated buffer zone in GCMs might focus on processes that form and expand the buffer zone.

Saravanan (1990) hypothesized that the buffer zone filters waves. Wave filtering means that the spectrum of waves entering the buffer zone differs from that exiting the buffer zone. Because of wave filtering, the buffer zone can influence the overall structure of the QBO. Using a zero-wind lower boundary condition imposes a buffer zone while neglecting wave filtering in the buffer zone. Because wave filtering depends on the mean flow, similar buffer zones will exhibit similar wave filtering. Because wave filtering is the main way the buffer zone affects the QBO, if two buffer zones have similar winds (even if they have different formation mechanisms), then the QBOs above those buffer zones will appear similar. Note how the QBOs are similar whether the buffer zone is expanded by upwelling (Fig. 1c), expanded by diffusivity (Fig. 7), or formed by mean-flow damping (Figs. 9b,c).

Aquila et al. (2014) used a GCM to simulate the response of the QBO to large stratospheric sulfate injections. The stratospheric sulfate injections invigorated the residual upwelling. For sufficiently large upwelling, the simulated QBO collapsed. The QBO in their model appears to have undergone period-lengthening collapse. (The hallmark of period-lengthening collapse is that the

QBO period lengthens without the QBO amplitude appreciably decreasing). The localized upwelling experiments studied here are not likely to be the strongest analog to the QBO behavior in the Aquila experiments, since their upwelling anomalies likely spanned the entire depth of the QBO region.

The response of the 1D model to dynamical perturbations depends on the type of perturbation, the location of the perturbation, the lower boundary condition, and the wave drag. We contrasted a wave drag formulation that had only critical-level dissipation (LH68) with a wave drag formulation that had wave dissipation below critical levels (P77). In the past decades, gravity wave parameterizations have proliferated, and are often introduced and tuned within GCMs to produce a QBO. Typically, half or more of the wave driving of simulated QBOs comes from parameterized gravity wave drag (Richter et al. 2014; Anstey et al. 2016; Garcia and Richter 2019). Simulated QBOs are typically interpreted in terms of the classical 1D model with either LH68 or P77 wave drag. However, having shown that QBO dynamics exhibit large sensitivity to the formulation of the wave drag (see also Campbell and Shepherd 2005a,b), efforts to interpret a GCM QBO in terms of the 1D model could benefit from using that GCM's gravity wave drag parameterization in the 1D model. Such efforts could help close the loop toward understanding the results of Schirber et al. (2015), who found that swapping gravity wave drag parameterizations in a GCM led to different QBO sensitivities to global warming.

Several terms in the 1D model serve as proxies for more complex three-dimensional dynamics. First, vertical diffusion is necessary in the 1D model to annihilate the stalled shear zone at the bottom of the domain (P77). Infinitesimal vertical diffusivity permits the annihilation of the stalled shear zone, but would lead to vertical shear far in excess of observed values. The vertical diffusivity used in 1D QBO studies is typically chosen to cap vertical shears near their observed maxima. Uncertainty remains regarding the processes for which the diffusion serves as a proxy, but it is not molecular diffusion and arguably represents the combined effects of small-scale turbulence and shear instabilities. The vertical diffusivity necessary to maintain realistic vertical shear exceeds that which is inferred from tracer patterns, such as the water vapor tape recorder, by a factor of 4–100 (Dunkerton 2000). The discrepancy between vertical diffusivity inferred from shears versus from tracers could be reconciled if the diffusivity varied in space and time, such as would be result from shear instabilities in zones of large shear (Mote et al. 1998; Dunkerton 2000). Second, we have argued that mean-flow damping is the only robust buffer zone formation mechanism (section 4). Whereas ion drag damps the mean flow in the ionosphere, there is, in principle, no expectation for mean-flow damping in the stratosphere. Although mean-flow damping is not expected from first principles, it serves as a proxy for stratospheric processes that effectively damp momentum anomalies, such as horizontal momentum flux divergence. Match and Fueglistaler (2019) diagnosed the effective mean-flow damping rate for each term in the relative angular momentum budget in the tropical stratosphere. Above the buffer zone, they diagnosed weak mean-flow damping, with damping time scales longer than the QBO time scale. In the buffer zone, they diagnosed mean-flow damping by horizontal momentum flux divergence on a time scale of 50 days, which could effectively damp the QBO winds. Third, the prescribed acceleration is used to represent the accelerations that lead to the semiannual oscillation.

Match and Fueglistaler (2019) suggested a possible analogy in the tropical stratosphere between tracer transport and the momentum flux divergence that leads to mean-flow damping. Just as mean-flow damping is weak in the active QBO region and strong in the buffer zone, lateral tracer transport is weak in the active QBO region and strong in the buffer zone (Plumb 1996; Mote et al. 1998; Haynes and Shuckburgh 2000; Dunkerton 2000). Additional tracer studies might help constrain the details of the mean-flow damping that forms the buffer zone.

The joint results of the 1D model and reanalyses implicate horizontal momentum flux divergence in forming the buffer zone. Horizontal momentum fluxes represent lateral exchange of momentum between the QBO and the far field atmosphere. By implicating lateral momentum exchange, the 1D QBO model has, for the purposes of producing a complete description of buffer zone formation, sown the seeds of its own obsolescence.

Further progress toward a complete theory for the buffer zone awaits higher-dimensional models, which would need to self-consistently include both vertical *and* horizontal momentum processes. However, in models with a self-consistent representation of the 3D dynamics, it is challenging to formulate experiments that test the QBO sensitivity to specific dynamical variables or processes. For example, because upwelling is part of the self-consistent circulation of a GCM, the sensitivity of the QBO to upwelling cannot be actively studied (i.e., by modifying the upwelling field) without violating either the self-consistency of the upwelling field or changing potentially confounding aspects of the flow. There is a trade-off between specificity (is upwelling the only variable changing?) and self-consistency (is upwelling changing in a way that preserves the internal consistency

between the upwelling field and the circulation as a whole?) Here, we have proposed a new hypothesis for buffer zone formation based on the 1D model, a model with maximum specificity of inference but zero self-consistency in its representation of upwelling, diffusivity, or damping. Because our mean-flow damping hypothesis replaces the upwelling hypothesis also based on the 1D model, the 1D model has, since 1990, provided the sole basis for hypotheses of buffer zone formation. Given the interpretive ease of the 1D model and the steep drop-off in the specificity of inference gained from models with even modest self-consistency, there is good reason to expect that the 1D model will remain central to hypotheses of buffer zone formation.

6. Conclusions

A buffer zone is a region where the QBO would exist were it not for dynamical interference by processes unrelated to the QBO (Match and Fueglistaler 2019). Using a 1D model of the QBO with a multiwave version of the P77 wave drag, Saravanan (1990) hypothesized that a buffer zone forms below a level where upwelling exceeds the wave-driven descent rate of the QBO. We have proposed a revised interpretation of the model experiments from Saravanan (1990).

Upwelling forms a buffer zone in the 1D model of the QBO with LH68 wave drag and in descent-rate models of the QBO with both LH68 and P77 wave drag. The models in which upwelling forms a buffer zone share the property that the wave drag acts like downward advection. Upwelling does not form a buffer zone in the 1D model with P77 wave drag, which has wave dissipation below critical levels and has wave drag that does not act like downward advection. When the P77 wave drag is used, upwelling can expand (but not form) a buffer zone, it can lead to period-lengthening collapse, or the QBO can simply reform below the upwelling. Just like upwelling, enhanced vertical diffusivity can also expand a preexisting buffer zone.

Mean-flow damping is the only dynamical perturbation that robustly forms a buffer zone, regardless of the location of the perturbation, lower boundary condition, or wave drag formulation. Because mean-flow damping forms the buffer zone, the zero-wind lower boundary condition typically used in classical QBO models tacitly assumes that mean-flow damping has produced a buffer zone. Match and Fueglistaler (2019) showed that, in reanalyses, horizontal momentum flux divergence effectively damps the mean flow in the buffer zone. Therefore, the zero-wind lower boundary condition implicitly represents lateral exchange of momentum between the QBO and the far-field atmosphere. The 1D model highlights the importance of such lateral momentum exchanges, although it cannot include them self-consistently. Future progress in understanding buffer zone formation that is complementary to the 1D theory described in this paper could be driven by constraints on momentum dynamics from tracer studies and judicious GCM experiments.

Acknowledgments. We thank Isaac Held for helpful discussions at various stages of this work. We thank Tim Dunkerton and two anonymous reviewers for their helpful comments, which improved this paper. This material is based upon work supported by the National Science Foundation Graduate Research Fellowship Program under Grant DGE-1656466. Any opinions, findings, and conclusions or recommendations expressed in this material are those of the authors and do not necessarily reflect the views of the National Science Foundation.

APPENDIX

1D Model

The QBO is driven by vertically propagating waves that interact with the mean flow. One-dimensional models (in altitude) are the minimal configurations that represent these wave–mean flow interactions, and these models facilitate understanding of the base state QBO and its response to dynamical perturbations. We analyze the following 1D model of the QBO:

$$\frac{\partial \overline{u}}{\partial t} = G + \frac{1}{\rho_0}\frac{\partial}{\partial z}\left(\rho_0 \nu \frac{\partial \overline{u}}{\partial z}\right) - \overline{w}^* \frac{\partial \overline{u}}{\partial z} - \kappa \overline{u} + X, \qquad \text{(A1)}$$

with wave drag G, diffusivity ν, density ρ_0, residual vertical velocity $\overline{w}^*$, mean-flow damping rate κ, and prescribed acceleration X. The terms on the right-hand side are wave drag, vertical diffusion, vertical advection, mean-flow damping, and prescribed acceleration. The wave drag G is a function of the modeled winds, whereas the prescribed acceleration X is independent of the winds and is used to impose a semiannual oscillation at the top of the domain when using the LH68 wave drag (which on its own cannot initiate new shear zones).

The model domain is from $z_L = 17$ km to $z_T = 37$ km. Subscript L refers to the lower boundary, and subscript T refers to the upper boundary. The model is solved numerically using the Crank–Nicolson method, an implicit scheme that is second order in space and time. The wave drag is formulated in a WKB sense where the waves are assumed to change much more rapidly than the mean wind (i.e., each time step), the wave drag is

computed as if the mean wind was constant. The vertical resolution $\Delta z = 250\,\text{m}$. Table 1 documents the physical parameter values used in the control simulations.

In the P77 wave drag formulation, the wave flux is solved on half levels. The incoming wave flux into the lowest model level is prescribed. If there is a critical layer (where $u = c$) between two levels, then the momentum flux into the higher level is set to zero, similar to the treatment in Saravanan (1990). The wave momentum flux divergence is computed by first-order difference.

Because advection in the Crank–Nicolson method is implicit, the LH68 wave drag is imposed as an effective vertical velocity, rather than as an explicit acceleration. Therefore, the effective vertical velocity due to the wave drag and prescribed vertical velocity operate identically.

The minimal configuration of the LH68 model includes a prescribed acceleration in the form of a semiannual oscillation X, which begins above 28 km and increases in amplitude with height:

$$X = \begin{cases} 0 & z < z_{\text{SA}} \\ 4\,\text{m s}^{-1}\left(\dfrac{z - z_{\text{SA}}}{1000\,\text{m}}\right)\omega_{\text{SA}}\cos(\omega_{\text{SA}} t) & z \geq z_{\text{SA}} \end{cases},$$

where $z_{\text{SA}} = 28\,\text{km}$, and $\omega_{\text{SA}} = 2\pi/180$ days.

REFERENCES

Anstey, J. A., J. F. Scinocca, and M. Keller, 2016: Simulating the QBO in an atmospheric general circulation model: Sensitivity to resolved and parameterized forcing. *J. Atmos. Sci.*, **73**, 1649–1665, https://doi.org/10.1175/JAS-D-15-0099.1.

Aquila, V., C. I. Garfinkel, P. Newman, L. Oman, and D. Waugh, 2014: Modifications of the quasi-biennial oscillation by a geoengineering perturbation of the stratospheric aerosol layer. *Geophys. Res. Lett.*, **41**, 1738–1744, https://doi.org/10.1002/2013GL058818.

Campbell, L. J., and T. G. Shepherd, 2005a: Constraints on wave drag parameterization schemes for simulating the quasi-biennial oscillation. Part I: Gravity wave forcing. *J. Atmos. Sci.*, **62**, 4178–4195, https://doi.org/10.1175/JAS3616.1.

——, and ——, 2005b: Constraints on wave drag parameterization schemes for simulating the quasi-biennial oscillation. Part II: Combined effects of gravity waves and equatorial planetary waves. *J. Atmos. Sci.*, **62**, 4196–4205, https://doi.org/10.1175/JAS3617.1.

Dunkerton, T. J., 1981: Wave transience in a compressible atmosphere. Part II: Transient equatorial waves in the quasi-biennial oscillation. *J. Atmos. Sci.*, **38**, 298–307, https://doi.org/10.1175/1520-0469(1981)038<0298:WTIACA>2.0.CO;2.

——, 1991: Nonlinear propagation of zonal winds in an atmosphere with Newtonian cooling and equatorial wave driving. *J. Atmos. Sci.*, **48**, 236–263, https://doi.org/10.1175/1520-0469(1991)048<0236:NPOZWI>2.0.CO;2.

——, 1997: The role of gravity waves in the quasi-biennial oscillation. *J. Geophys. Res.*, **102**, 26 053–26 076, https://doi.org/10.1029/96JD02999.

——, 2000: Inferences about QBO dynamics from the atmospheric "tape recorder" effect. *J. Atmos. Sci.*, **57**, 230–246, https://doi.org/10.1175/1520-0469(2000)057<0230:IAQDFT>2.0.CO;2.

——, and D. P. Delisi, 1997: Interaction of the quasi-biennial oscillation and stratopause semiannual oscillation. *J. Geophys. Res.*, **102**, 26 107–26 116, https://doi.org/10.1029/96JD03678.

Garcia, R. R., and J. H. Richter, 2019: On the momentum budget of the quasi-biennial oscillation in the Whole Atmosphere Community Climate Model. *J. Atmos. Sci.*, **76**, 69–87, https://doi.org/10.1175/JAS-D-18-0088.1.

Geller, M. A., and Coauthors, 2016: Modeling the QBO-improvements resulting from higher-model vertical resolution. *J. Adv. Model. Earth Syst.*, **8**, 1092–1105, https://doi.org/10.1002/2016MS000699.

Gray, L. J., and J. A. Pyle, 1989: A two-dimensional model of the quasi-biennial oscillation of ozone. *J. Atmos. Sci.*, **46**, 203–220, https://doi.org/10.1175/1520-0469(1989)046<0203:ATDMOT>2.0.CO;2.

Hamilton, K., R. J. Wilson, and R. S. Hemler, 1999: Middle atmosphere simulated with high vertical and horizontal resolution versions of a GCM: Improvements in the cold pole bias and generation of a QBO-like oscillation in the tropics. *J. Atmos. Sci.*, **56**, 3829–3846, https://doi.org/10.1175/1520-0469(1999)056<3829:MASWHV>2.0.CO;2.

Hampson, J., and P. Haynes, 2004: Phase alignment of the tropical stratospheric QBO in the annual cycle. *J. Atmos. Sci.*, **61**, 2627–2637, https://doi.org/10.1175/JAS3276.1.

Haynes, P., and E. Shuckburgh, 2000: Effective diffusivity as a diagnostic of atmospheric transport: 2. Troposphere and lower stratosphere. *J. Geophys. Res.*, **105**, 22 795–22 810, https://doi.org/10.1029/2000JD900092.

Holton, J. R., and R. S. Lindzen, 1972: An updated theory for the quasi-biennial cycle of the tropical stratosphere. *J. Atmos. Sci.*, **29**, 1076–1080, https://doi.org/10.1175/1520-0469(1972)029<1076:AUTFTQ>2.0.CO;2.

Kawatani, Y., and K. Hamilton, 2013: Weakened stratospheric quasibiennial oscillation driven by increased tropical mean upwelling. *Nature*, **497**, 478–481, https://doi.org/10.1038/nature12140.

——, ——, and S. Watanabe, 2011: The quasi-biennial oscillation in a double CO_2 climate. *J. Atmos. Sci.*, **68**, 265–283, https://doi.org/10.1175/2010JAS3623.1.

Lindzen, R. S., and J. R. Holton, 1968: A theory of the quasi-biennial oscillation. *J. Atmos. Sci.*, **25**, 1095–1107, https://doi.org/10.1175/1520-0469(1968)025<1095:ATOTQB>2.0.CO;2.

Martin, Z., S. Wang, J. Nie, and A. Sobel, 2019: The impact of the QBO on MJO convection in cloud-resolving simulations. *J. Atmos. Sci.*, **76**, 669–688, https://doi.org/10.1175/JAS-D-18-0179.1.

Match, A., and S. Fueglistaler, 2019: The buffer zone of the quasi-biennial oscillation. *J. Atmos. Sci.*, **76**, 3553–3567, https://doi.org/10.1175/JAS-D-19-0151.1.

McIntyre, M. E., 1994: The quasi-biennial oscillation (QBO): Some points about the terrestrial QBO and the possibility of related phenomena in the solar interior. *The Solar Engine and Its Influence on Terrestrial Atmosphere and Climate*, E. Nesme-Ribes, Ed., Springer, 293–320, https://doi.org/10.1007/978-3-642-79257-1_18.

Mote, P. W., T. J. Dunkerton, M. E. McIntyre, E. A. Ray, P. H. Haynes, and J. M. Russell, 1998: Vertical velocity, vertical diffusion, and dilution by midlatitude air in the tropical lower stratosphere. *J. Geophys. Res.*, **103**, 8651–8666, https://doi.org/10.1029/98JD00203.

Plumb, R. A., 1977: The interaction of two internal waves with the mean flow: Implications for the theory of the quasi-biennial oscillation. *J. Atmos. Sci.*, **34**, 1847–1858, https://doi.org/10.1175/1520-0469(1977)034<1847:TIOTIW>2.0.CO;2.

——, 1996: A "tropical pipe" model of stratospheric transport. *J. Geophys. Res.*, **101**, 3957–3972, https://doi.org/10.1029/95JD03002.

Rajendran, K., I. M. Moroz, P. L. Read, and S. M. Osprey, 2016: Synchronisation of the equatorial QBO by the annual cycle in tropical upwelling in a warming climate. *Quart. J. Roy. Meteor. Soc.*, **142**, 1111–1120, https://doi.org/10.1002/qj.2714.

——, ——, S. M. Osprey, and P. L. Read, 2018: Descent rate models of the synchronization of the quasi-biennial oscillation by the annual cycle in tropical upwelling. *J. Atmos. Sci.*, **75**, 2281–2297, https://doi.org/10.1175/JAS-D-17-0267.1.

Richter, J. H., A. Solomon, and J. T. Bacmeister, 2014: On the simulation of the quasi-biennial oscillation in the Community Atmosphere Model, version 5. *J. Geophys. Res. Atmos.*, **119**, 3045–3062, https://doi.org/10.1002/2013JD021122.

——, and Coauthors, 2020: Response of the quasi-biennial oscillation to a warming climate in global climate models. *Quart. J. Roy. Meteor. Soc.*, https://doi.org/10.1002/qj.3749, in press.

Saravanan, R., 1990: A multiwave model of the quasi-biennial oscillation. *J. Atmos. Sci.*, **47**, 2465–2474, https://doi.org/10.1175/1520-0469(1990)047<2465:AMMOTQ>2.0.CO;2.

Schenzinger, V., S. Osprey, L. Gray, and N. Butchart, 2017: Defining metrics of the quasi-biennial oscillation in global climate models. *Geosci. Model Dev.*, **10**, 2157–2168, https://doi.org/10.5194/gmd-10-2157-2017.

Schirber, S., E. Manzini, T. Krismer, and M. Giorgetta, 2015: The quasi-biennial oscillation in a warmer climate: Sensitivity to different gravity wave parameterizations. *Climate Dyn.*, **45**, 825–836, https://doi.org/10.1007/s00382-014-2314-2.

Yoo, C., and S.-W. Son, 2016: Modulation of the boreal wintertime Madden-Julian oscillation by the stratospheric quasi-biennial oscillation. *Geophys. Res. Lett.*, **43**, 1392–1398, https://doi.org/10.1002/2016GL067762.